Journal of Nuclear Materials 415 (2011) S400–S404

Contents lists available at ScienceDirect

Journal of Nuclear Materials

journal homepage: www.elsevier.com/locate/jnucmat

NSTX plasma response to lithium coated divertor

H.W. Kugel [a,*], M.G. Bell [a], J.P. Allain [b], R.E. Bell [a], S. Ding [c], S.P. Gerhardt [a], M.A. Jaworski [a], R. Kaita [a], J. Kallman [a], S.M. Kaye [a], B.P. LeBlanc [a], R. Maingi [d], R. Majeski [a], R. Maqueda [a], D.K. Mansfield [a], D. Mueller [a], R. Nygren [e], S.F. Paul [a], R. Raman [f], A.L. Roquemore [a], S.A. Sabbagh [g], H. Schneider [a], C.H. Skinner [a], V.A. Soukhanovskii [h], C.N. Taylor [b], J.R. Timberlake [a], W.R. Wampler [e], L.E. Zakharov [a], S.J. Zweben [a], the NSTX Research Team

[a] Princeton Plasma Physics Laboratory, Princeton, NJ 08543, USA
[b] Purdue University, West Lafayette, IN 47907, USA
[c] Academy of Science Institute of Plasma Physics, Hefei, China
[d] Oak Ridge National Laboratory, Oak Ridge, TN 37831, USA
[e] Sandia National Laboratories, Albuquerque, NM 87185, USA
[f] University of Washington, Seattle, WA 98195, USA
[g] Columbia University, New York, NY 10027, USA
[h] Lawrence Livermore National Laboratory, Livermore, CA 94551, USA

ARTICLE INFO

Article history:
Available online 15 December 2010

ABSTRACT

NSTX experiments have explored lithium evaporated on a graphite divertor and other plasma-facing components in both L- and H- mode confinement regimes heated by high-power neutral beams. Improvements in plasma performance have followed these lithium depositions, including a reduction and eventual elimination of the HeGDC time between discharges, reduced edge neutral density, reduced plasma density, particularly in the edge and the SOL, increased pedestal electron and ion temperature, improved energy confinement and the suppression of ELMs in the H-mode. However, with improvements in confinement and suppression of ELMs, there was a significant secular increase in the effective ion charge Z_{eff} and the radiated power in H-mode plasmas as a result of increases in the carbon and medium-Z metallic impurities. Lithium itself remained at a very low level in the plasma core, <0.1%. Initial results are reported from operation with a Liquid Lithium Divertor (LLD) recently installed.

1. Introduction

The National Spherical Torus Experiment (NSTX) [1,2] has been investigating lithium (Li) evaporated on its plasma-facing components (PFCs) for density and impurity control [2–5]. This research with lithium applied to graphite surfaces with temperatures in the range 30–50 °C (*i.e.*, below lithium melting temperature of 180 °C) has been a prelude to using liquid lithium to control density, edge collisionality, impurity influxes.

Lithium evaporated on graphite has the potential for control of density due to its ability to absorb the atomic and ionic deuterium efflux through formation of complex chemical bonds which sequester deuterium, making it unavailable for recycling [6,7]. Due to the range of deuterium in lithium (<250 nm [8]), the intercalation of lithium into NSTX graphite [9], and the immobility of the lithium compounds formed in graphite, the absorption can saturate in the near surface layer [8,9], limiting the deuterium pumping capability of lithium evaporated on graphite. Due to these effects, these lithium depositions can provide only short pulse capability, and subsequent recoating between NSTX discharges is required to replenish the surface with fresh lithium. Liquid lithium on the other hand has a much higher capacity for sequestering deuterium [10] because lithium-deuteride is more mobile in liquid lithium. In addition, it also has potential for handling high power fluxes, and liquid surfaces are self-healing after high-power transients [11].

2. Results using lithium evaporated on graphite divertor tiles

NSTX has been evaporating lithium on graphite tiles of the lower divertor region since 2007 [2–5]. Typically the graphite tile bulk temperatures are in the range 30–50 °C. Fig. 1 shows a schematic diagram of the poloidal cross section of NSTX, and the locations of two LIThium Evaporators (LITERs) at toroidal angles 165° and 315°, and the LITER central axes aimed at the lower divertor. The shaded regions indicate the measured half-angle of

* Corresponding and Presenting author. Address: PPPL, P.O. Box 451, Princeton NJ 08543, USA.
E-mail address: hkugel@pppl.gov (H.W. Kugel).

0022-3115/$ - see front matter © 2010 Elsevier B.V. All rights reserved.
doi:10.1016/j.jnucmat.2010.12.016

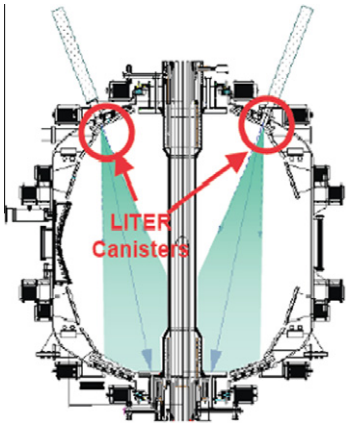

Fig. 1. Schematic diagram of the poloidal cross section of NSTX, showing the locations of the two LIThium EvaporatoRs (LITERs) at toroidal angles 165° and 315°, and the LITER central axes aimed at the lower divertor. The shaded regions indicate the measured half-angle of the roughly Gaussian measured angular distribution of the lithium vapor plume at the 1/e intensity.

the roughly Gaussian measured angular distribution at the 1/e intensity of the vapor plume emerging from the exit duct. A rotatable lithium shutter is positioned in front of each LITER output aperture to stop the lithium vapor stream from reaching plasma-facing components when the diagnostic window shutters are open during a discharge [5]. This capability also allows lithium deposition to be stopped for a sequence of discharges. This is done to establish "pre-lithium wall conditions", for reference discharges by allowing the plasma deuterium efflux to be absorbed by previously deposited active lithium coatings. This efflux saturates the lithium coating within about 2 discharges, and renders it unable to pump via the formation of LiD [4,5].

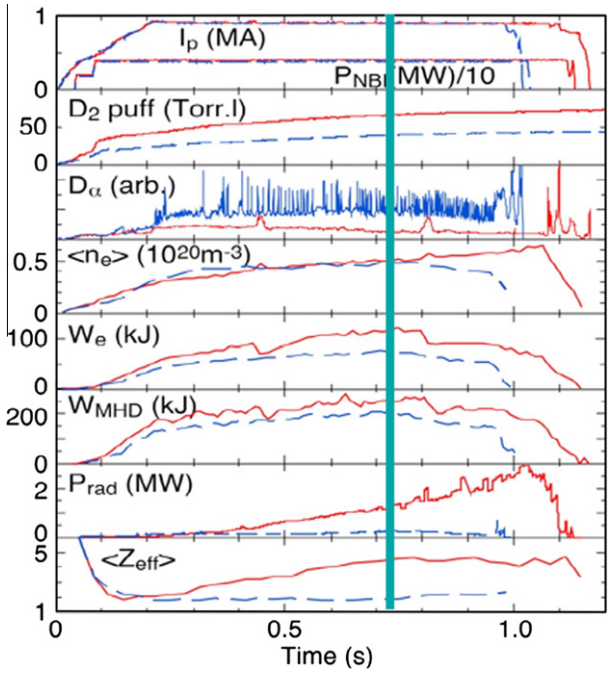

Fig. 2. Reference waveforms pre-lithium wall conditions, *i.e.* saturated lithium conditions with no pumping established by closing the lithium shutters and allowing the lithium coating to saturate (129239, blue), and after applying a 260 mg fresh lithium deposition with the lithium shutters open (129245, red), deuterium recycling was reduced, ELMs were suppressed, and confinement improved. The vertical line at 0.72 s is the time reference for Fig. 3.

In 2009, the LITERs provided evaporated lithium depositions immediately before the majority of discharges. Shown in Fig. 2 are typical waveforms for pre-lithium wall conditions, *i.e.*, no active pumping lithium as obtained with the lithium shutters closed (blue) and with the lithium shutters open (red). After a 260 mg fresh lithium deposition (red), the deuterium gas puffing required to achieve a similar average density was increased although the deuterium Balmer-α line emission (Dα) was lower, indicating reduced deuterium recycling, ELMs were suppressed, and confinement improved, as indicated by the increases in total and electron stored energy. Note, however, that with improved confinement and without ELMs, impurity accumulation increased radiated power and Z_{eff}. Quantitative measurements of C^{6+}, Li^{3+} with charge-exchange recombination spectroscopy indicate that the carbon-to-lithium density ratio was 30–100 in the core of the plasma [2]. It is possible to eliminate this impurity accumulation by introducing controlled ELMs via application of pulses of non-axisymmetric radial field perturbations [12].

Shown in Fig. 3 are the radial profiles for the discharges shown in Fig. 2 obtained with the lithium shutters closed and all lithium deposition saturated (blue) and after 260 mg of fresh lithium deposition with lithium shutters open (red) at the time reference 0.72 s. The radial density and temperature profiles indicate that the transition to a lithium-coated wall produced a higher temperature, lower density plasma edge. Noteworthy is the reduction in D_α luminosity, an indicator of recycling reduction, across the lower divertor surface as the lithium deposition increased from zero initially (Fig. 4).

The increase in plasma stored energy (Fig. 2) is mostly in the electron channel. Fig. 5 compares the central electron temperature and volume averaged electron temperature between ensembles of otherwise similar discharges for pre-lithium (*i.e.,* no active pumping lithium) and active lithium conditions. The improved electron confinement, the broadening of the electron temperature profile, and the elimination of ELMs occur with the observed reduction in edge fueling resulting from lithium edge conditions. The time dependent transport analysis code TRANSP [13] results (Fig. 6) confirm that electron thermal transport is progressively reduced as lithium deposition increases [14]. In addition, the fast-ion contribution to total energy increased. The thermal ion confinement remains close to the neoclassical level, both with and without lithium.

Analysis of the data suggests that modification of the plasma density profile by lithium edge pumping changes ELM stability, as previously predicted [15]. The lithium edge conditions reduce recycling and edge fueling. Consequently, the edge density decreases, and although the edge temperature increases, the peak edge pressure gradient is shifted inwards in minor radius where the magnetic shear is lower. As test of the applicability of the PEST ideal MHD code [16] and ELITE ideal MHD code [17,18] to the observed ELM behavior, these codes were applied to the analysis of the normalized edge current and normalized edge pressure gradient. The results indicate that NSTX pre-lithium (*i.e.,* no active pumping lithium) edge profiles are close to the kink/peeling instability threshold [19], whereas the post-lithium cases are stable to these modes [19]. The PEST results which indicate instability of low-n modes are consistent with our previous observations of low $n = 1$–5 pre-cursor oscillations before the ELM crash in NSTX [19].

3. PFC conditions following lithium evaporation on graphite divertor tiles

Evaporated lithium depositions consistently and promptly restore good operational conditions in NSTX without boronization,

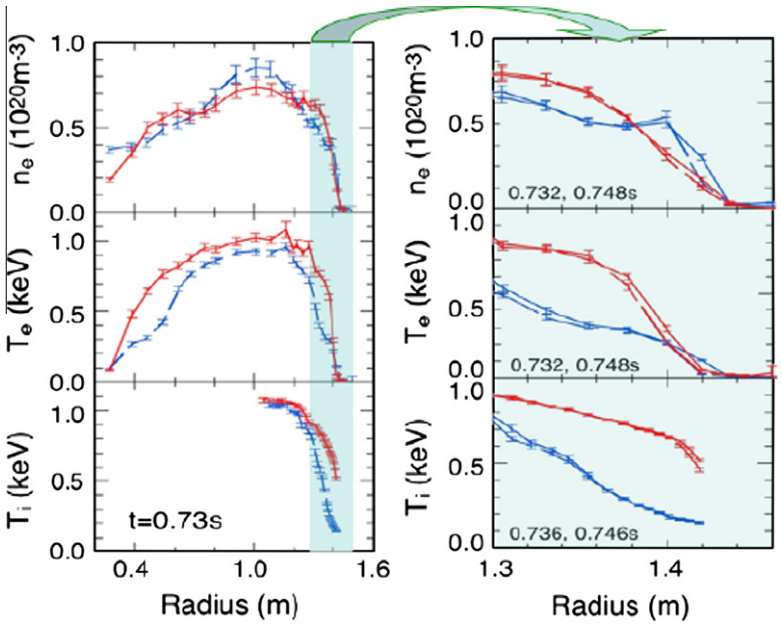

Fig. 3. Measured radial profiles of the plasma density and temperatures for discharges shown in Fig. 2 before (blue) and after 260 mg lithium deposition (red) at discharge time 0.72 s (vertical line in Fig. 2) for pre-lithium wall conditions, *i.e.*, saturated lithium conditions with no pumping established by closing the LITER lithium shutters and allowing the lithium coating to saturate.

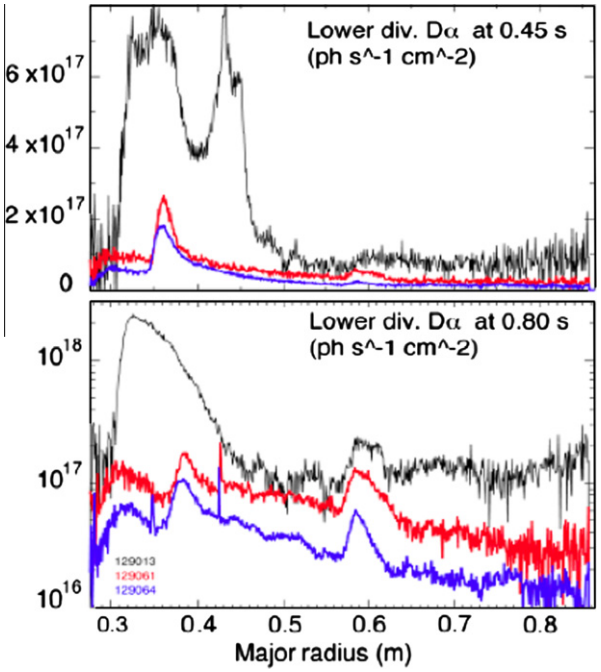

Fig. 4. Radial profiles and reduction in D_α luminosity, an indicator of recycling reduction, as the lower divertor plasma facing surface was progressively covered with lithium. Shown are profiles at (a) 0.45 s and (b) 0.8 s.

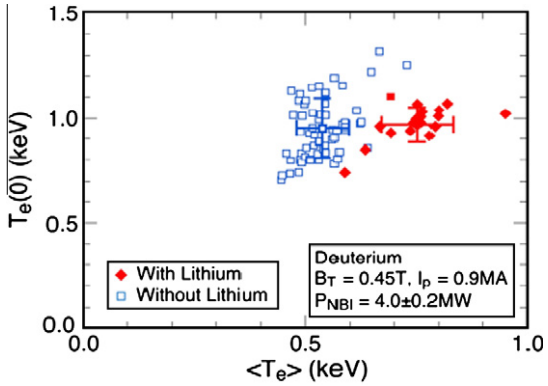

Fig. 5. Central electron temperature versus volume averaged electron temperature for an ensemble of plasmas without lithium and with evaporated lithium deposition on the PFCs under otherwise similar conditions.

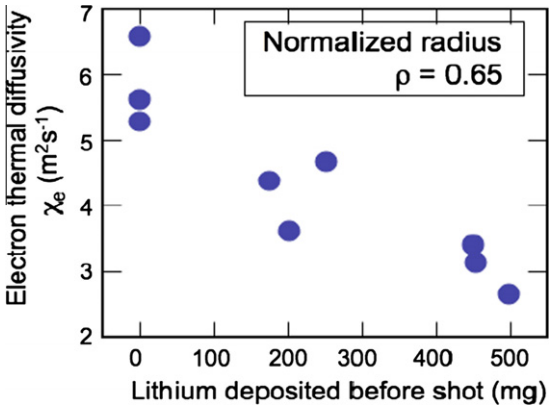

Fig. 6. The transport analysis code TRANSP results for the electron thermal diffusivity as lithium deposition was increased with other discharges held constant.

including following vacuum vents to atmosphere. With a typical base pressure in the range of 3–5 $\times$ 10^{-8} torr, the deposited lithium reacts only slowly with the residual vacuum constituents (H_2O, CO, CO_2) to form lithium compounds containing oxygen, predominantly LiOH, and to a lesser extent Li_2O and Li_2CO_3 [6]. After a typical annual 12–18 week experimental campaign, NSTX is vented to atmosphere, and purged with humidified air for at least 1 week prior to the personnel entry. This venting procedure converts any residual active lithium and LiOH to mostly inert Li_2CO_3.

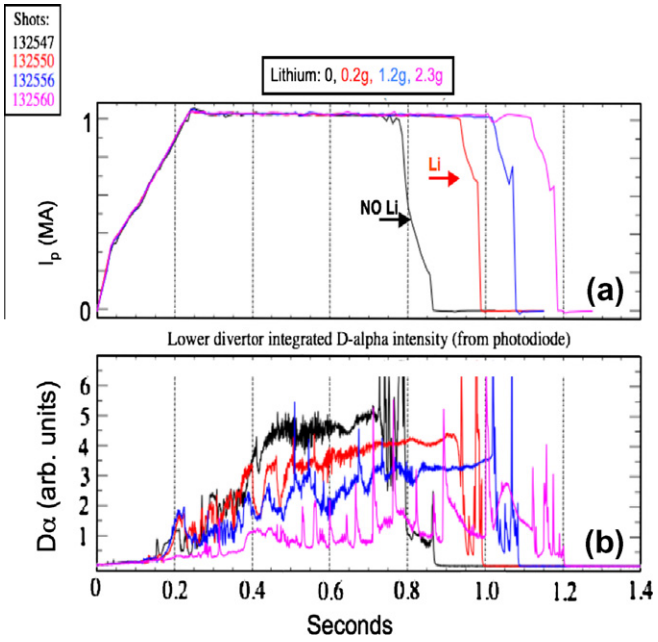

Fig. 7. Lithiumization promptly restored good operational conditions without boronization. The application of 2.3 g of lithium following plasmas with high oxygen content resulted in significantly (a) extending pulse duration, and (b) reducing edge recycling as indicated by the deuterium Balmer-α line emission.

At the beginning of operation in 2009, the walls remained coated with some residual Li_2CO_3 after the preceding vent for installation of diagnostics and maintenance. Following bakeout and boronization with deuterated trimethylboron (TMB), plasmas exhibited a reduced pulse length which was believed to be due to this contamination. After 6 weeks of discharge conditioning, and argon, neon, and helium glow-discharge cleaning, initial plasmas still exhibited reduced pulse length. However, after a 2.3 g lithium deposition, good operational conditions were restored in less than 10 discharges (Fig. 7). In 2010, prior to evacuation, all the plasma-facing graphite surfaces were cleaned with an abrasive pad and all exposed surfaces, both graphite and metallic, were washed with a 5% solution of acetic acid (common vinegar) to convert Li_2CO_3 to water-soluble lithium acetate ($LiC_2H_3O_2$) so it could be removed on damp lint-free cloths. Finally, all surfaces were washed with deionized water and ethanol. After evacuation, a 3 week vessel vacuum bake was performed, and following this, a 12 g evaporated lithium deposition was applied (without boronization). Within a few hours of the first discharge, extended H-mode discharges were produced with neutral beam heating.

4. Initial results using liquid lithium divertor

Motivated by the potential benefits of liquid lithium as a plasma facing surface, NSTX has started to test a Liquid Lithium Divertor (LLD) for integrating high plasma performance with solutions to the challenges of plasma surface interactions. Shown in Fig. 8 is a photo of the LLD installed prior to the start of operation in 2010. The LLD consists of four heated metal plates, each spanning 80° toroidally, which replace a 20 cm wide annulus of the graphite tiles on the conical outer divertor [20,21]. The plasma facing surface is a 0.165 mm thick layer of molybdenum plasma-sprayed with a 45% porosity onto a 0.25 mm thick stainless steel barrier brazed to a 22.2 mm thick copper base-plate. The molybdenum porosity is intended to make the lithium surface tension forces large relative to electromagnetic forces in the liquid layer. The molybdenum porosity of 45% was estimated from microscopic image analysis

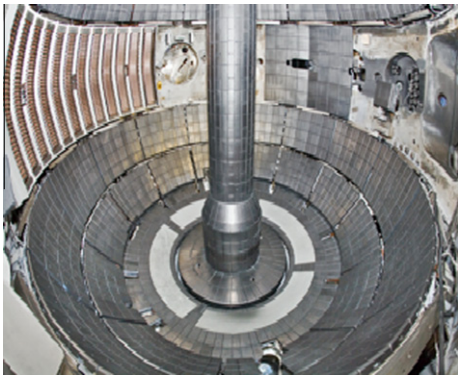

Fig. 8. Photo of the NSTX Liquid lithium Divertor (LLD-1) installed in 2010 near the inner edge of the outer divertor. It consists of four 80° toroidal sections, each 20 cm wide in the radial direction. Each section is separated by a row of graphite diagnostic tiles containing magnetic sensors, thermocouples, Langmuir probes, and bias electrodes.

of the coating cross-sections. This image analysis also indicated that the voids in this porosity are of order 10 μm. The pore size is large compared to that of the surrounding graphite tiles for which electron microscopic images indicate that the pore size is less than 0.1 μm. The thin stainless steel serves as a barrier to prevent liquid lithium from reacting with the copper substrate. Each plate is supported at its corners by the divertor baseplate with fasteners providing structural support, electrical isolation, and allowing thermal expansion. Each is electrically grounded to vessel at one mid-segment location to reduce eddy currents and to measure via a Rogowski coil "halo currents" entering the plate from the plasma. Electrical heaters and gas cooling lines are used to maintain a surface temperature in the range 20 –400 °C. Between the sectors toroidally, graphite tiles are mounted containing diagnostics and bias electrodes. For the experiments in 2010, the LLD and the lower divertor graphite PFCs are being coated with lithium using the LITER units. Later LLD embodiments may involve a flowing lithium fill system.

The LLD is expected to provide pumping, not only when the outer strike point is directly on the LLD, but also when it is inboard of the LLD. This is due to the high flux expansion factor (15–20) in NSTX between the SOL at the outboard midplane and at the divertor surface. The capability to apply this range of diverted discharge configurations will test the potential benefits of liquid lithium divertor for integrating high plasma and PSI performance. In particular, it will test the capability of broad-area pumping to reduce plasma density and thereby increase neutral beam current drive to achieve advanced discharge scenarios in NSTX.

The initial lithium depositions on the LLD with the LITER system were performed with 3 of the 4 LLD plates varied in bulk average temperature from ambient to 320 °C (the melting point of lithium is 180 °C). The bulk average temperatures of the LLD plates were measured by an array of 32 type-K thermociouples per plate; IR camera temperature measurements of the front face temperatures of the plates were unavailable. During this intial work, the 4th plate was at room temperature. The LITER system was used to deposit lithium over the entire lower divertor region (spanning the major radius from 0.35 m to 1.1 m) which includes the graphite tiles and all 4 plates of the LLD (spanning the major radius from 0.65 m to 0.85 m). Evaporation at a total rate of 20–40 mg/min was used. The initial depositions were applied before plasma operation started. Visible camera images of the plates during this initial loading indicated that lithium was absorbed into the porous molybdenum front face of the LLD. The unheated plate exhibited higher reflectivity than the heated plates as lithium soaked into the surface of the heated plates. It was estimated that the porous

molybdenum layer on the LLD was filled to about 5% of its total capacity over several weeks. This estimate was done using a simulation of the LITER deposition efficiency over the region of the LLD base using the measured angular distribution of lithium emission from LITER [5]. No other method was available to determine the amount of lithium deposited on the LLD. The results of spectroscopic views of the LLD region were used to indicate relative changes in D_α and lithium luminosities are under analysis. Possible Mo, Fe, and Cu luminosities from LLD materials were also monitored but not observed. When plasma operation started, reproducible, ELM-free, H-mode discharges were obtained with the diverted outer strike point at major radii ranging from the inner divertor out to the LLD. These ELM-free, H-mode discharges with neutral beam heating of 2–6 MW exhibited reproducibly higher energy confinement times and reduced flux consumption early in these discharges relative to pre-lithium, *i.e.,* saturated lithium conditions with no pumping. However, in these initial experiments, little pumping difference was measured compared to previous evaporated lithium depositions over the same region prior to installation of LLD. The LLD diagnostics are functioning, including thermocouples embedded in the LLD plates, the halo current sensors, other magnetic sensors, and an array of 99 Langmuir probes in one of the graphite tiles between the LLD plates designed to measure edge temperature, density, and electric potential.

5. Discussion

NSTX experiments with lithium evaporated on the graphite divertor tiles have demonstrated an increased plasma current pulse length relative to the pre-lithium reference discharges (*i.e.* saturated lithium conditions with no pumping), earlier H-mode transitions, significant density reduction in the early part of discharges, requiring more fueling early to avoid deleterious MHD activity, increased electron temperature, electron stored energy and confinement time, and reduced OV/CIII impurity ratios [5]. As the evaporated lithium deposition thickness increased, high elongation H-mode discharges became ELM-free. Eventually the HeGDC previously routinely employed between plasma shots, was eliminated, allowing an increased duty cycle.

Initial experiments have been performed with a recently installed liquid lithium divertor (LLD) module. Edge pumping by the combination of the LLD, about 5% filled, and the evaporated lithium deposition on the graphite tiles exhibited little difference compared to previous evaporated lithium depositions over the same region prior to installation of LLD. This can be understood, if the initial efflux incident on active evaporated lithium deposition on the graphite tiles and on the liquid lithium in the LLD results in comparable sequestration of the incident deuterium (7). Post-discharge heating of the LLD plates showed an increase in deuterium partial pressure consistent with thermal desorption studies of hydrated lithium [10]. Since, in NSTX, lithium evaporated on the graphite divertor tiles saturates in about 1–2 discharges, its pumping effect can in effect be turned-off by ceasing to replenishment with evaporation between discharges. Hence, the next step in this work is to fill the LLD to about 50% of its capacity, then turn-off LITER evaporation to let the evaporated lithium deposition saturate. Under these conditions the resulting effects should be due predominantly to the liquid LLD.

More than a decade of research has pointed to the merits and potential reactor relevance of replenishable liquid lithium walls for providing a pumping, impurity flushing, low-*Z*, self-healing plasma facing surface [11,22,23]. Additional work is needed to investigate if liquid lithium can produce and integrate four important potential benefits for fusion: (a) divertor pumping over large surface area compatible with high flux expansion solutions for power exhaust and low collisionality, (b) improved confinement, (c) ELM reduction and elimination, and (d) high-heat flux handling, e.g., via capillary flow. NSTX lithium experiments are the first extension of this work to high beta, high power, long pulse, NBI conditions in a spherical torus.

Acknowledgments

This work is supported by United States Department of Energy (US DOE) Contracts DE-AC02-09CH11466 (PPPL), DE-AC05-00OR22725 (ORNL), and DE-AC52-07NA27344 (LLNL), and that of Sandia, a multi-program laboratory operated by Lockheed Martin Company, for the United States Department of Energy's National Nuclear Security Administration, under contract DE-AC04-94AL85000.

References

[1] M. Ono et al., Nucl. Fusion 40 (2000) 557.
[2] M.G. Bell et al., Plasma Phys. Control. Fus. 51 (2009) 124056.
[3] H.W. Kugel et al., J. Nucl. Mater. 363–365 (2007) 791.
[4] H.W. Kugel et al., Phys. Plasmas 15 (2008) 056118.
[5] H.W. Kugel et al., J. Nucl. Mater. 390–391 (2009) 1000.
[6] J.P. Allain et al., J. Nucl. Mater. 390–391 (2009) 942.
[7] C.N. Taylor et al., in this Conference.
[8] J.N. Brooks et al., J. Nucl. Mater. 337–339 (2005) 1053.
[9] W.R. Wampler et al., J. Nucl. Mater. 390–391 (2009) 1009.
[10] M.J. Baldwin et al., Nucl. Fusion 42 (2002) 1318.
[11] V.A. Evtikhin et al., Plasma Phys. Control Fusion 44 (2002) 955. and references therein..
[12] J.M. Canik et al., Phys. Rev. Lett 104 (2010) 045001.
[13] R.J. Hawryluk, in: B. Coppi et al. (Eds.), Physics of Plasmas Close to Thermonuclear Conditions, vol. 1, CEC, Brussels, 1980, pp. 19–46.
[14] S. Ding et al., Plasma phys. Control. Fusion 52 (2010) 015001.
[15] L.E. Zakharov et al., J. Nucl. Mater. 363–365 (2007) 453.
[16] R. Grimm et al., Methods Comput. Phys. 16 (1976) 253.
[17] P.B. Snyder et al., Phys. Plasmas 9 (2002) 2037.
[18] H.R. Wilson et al., Phys. Plasmas 9 (2002) 1277.
[19] R. Maingi et al., Phys. Rev. Lett. 103 (2009) 075001.
[20] H.W. Kugel et al., Fusion Eng. Des. 84 (2009) 1125.
[21] R.E. Nygren et al., Fusion Eng. Des. 84 (2009) 1438.
[22] M. Abdou et al., Fus. Eng. Design 72 (2004) 1. and references therein.
[23] S.V. Mirnov et al., 390–391 (2009) 876.